In Orbit Performance and Calibration of the Rossi X-ray Timing Explorer (RXTE) Proportional Counter Array (PCA)

K. Jahoda, J. H. Swank, A. B. Giles, M. J. Stark, T. Strohmayer, W. Zhang

Laboratory for High Energy Astrophysics, Code 662
Goddard Space Flight Center
Greenbelt, MD 20771

E. H. Morgan

Center for Space Research, MIT
Cambridge, MA 02139

July 9, 1996

ABSTRACT

The Proportional Counter Array (PCA) is designed to perform μ-second timing of bright galactic sources and broad band, confusion limited, studies of faint extragalactic sources in the 2-60 keV X-ray band. The PCA was launched as part of the Rossi X-ray Timing Explorer (RXTE) satellite into a circular orbit of altitude 580 km and 23° inclination on December 30, 1995. The mission contains three experiments: a set of large area Xenon proportional counters sensitive from $2-60$ keV (Proportional Counter Array: PCA), a set of large area sodium iodide scintillators sensitive from $15-200$ keV (High Energy X-ray Timing Experiment: HEXTE), and three wide field of view scanning detectors which monitor most of the sky each orbit (All Sky Monitor: ASM). The goals of the mission are summarized by Swank et al.[1] We present performance and calibration data on the measured and predicted in-orbit background, energy response, relative and absolute timing performance, and the operational possibililities made available with the high performance Experiment Data System (EDS) designed and built by MIT.

Keywords: Proportional Counters, on-orbit performance, timing, background

1 PCA DESCRIPTION

The PCA consists of 5 large, nearly identical, proportional counter units (PCUs).[2,3] Each detector has an effective area of $\sim 1300\,\mathrm{cm}^2$ defined by a hexagonal collimator of beryllium copper. The nominal thickness of each sheet of the collimator is 2.7 mil; the depth of the collimator is 8 inches and the dimension of each cell is 0.125 inch measured flat to flat.

Behind the collimator two mylar windows, each 1 mil thick and coated on both sides with 700 angstroms of aluminum and separated by 1.3 cm, define a gas volume filled with Propane (nominally to 802 torr at 22° C). Behind the second window the main volume is filled with a Xenon/Methane (90/10) mixture nominally filled to 840 torr. The signal anodes are grouped into six signal chains, each of which consists of alternate anodes within a single layer.[2] There are separate signal chains for the propane anodes, the outermost anodes (veto anodes), and for a calibration flag. An exploded view is shown in Zhang et al.[3]

Each anode chain has individual discriminators, preamplifier and shaping amplifier; the six signal anodes and propane anodes within each PCU share a single Analog to Digital converter which produces an 8 bit pulse height. The veto chain produces a 2 bit pulse

height through discriminators. Each time an event is processed, a 19 bit stream is generated and passed to the Experiment Data System (EDS) for processing and possible compression for telemetry. The bit stream contains the pulse height (8 bits), the veto chain pulse height (2 bits), lower level discriminators (LLD) for the signal, propane, and calibration chains (8 bits), and a Very Large Event (VLE) flag (1 bit) which indicates that one of the shaping amplifiers was driven into saturation and that event processing has been suspended for a commandable length of time. If only one LLD is present (or the calibration and one other LLD) the origin of the event is specified. If 2 or more LLDs are present, the pulse height is ambiguous. This is discussed further in the sections on Timing and Energy.

The EDS performs user selected compression of the event data in order to keep the average telemetry below 40 kbps. (The Spacecraft memory can support intervals of up to 30 minutes at instantaneous telemetry rates up to $\sim$ 300 kbps.) Most modes are designed with the assumption that good events (i.e. x-rays) will have exactly one discriminator bit set and that all of the multiple discriminator events are a background due to charged particles. In the limiting cases of high rates, the events with 2 LLDs (and even 3 LLDs) are dominated by coincidences of multiple cosmic events being detected on different signal chains.

Timing information and PCU identification are supplied by the EDS on receipt of the event; the delay between the LLD threshold being exceeded and the application of an EDS time-tag has been measured on the ground to be 18μs. This value is constant for given pulse height, but goes down to 15μs for events just at the discriminator threshold.

2 ON BOARD PROCESSING

The PCA has two standard processing modes which run all the time in addition to the modes selected by Guest Observers. Standard 1 contains 8 rates sampled at 0.125 sec: the total good event rate from each individual counter, the propane event rates summed over the PCA, the very large event rate summed over the PCA, and the rate of all other events. Standard 1 also contains calibration spectra which are stored and telemetered separately for each detector and each layer once every 128 seconds. Standard 2 contains 129 channel pulse height spectra for each signal layer of each detector, 33 channel propane layer spectra for each detector, and 29 rates of various combinations of coincidences for each detector read out every 16 seconds.[4]

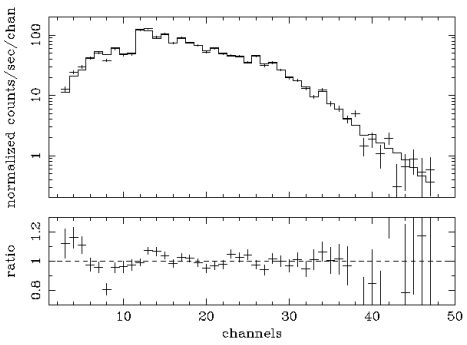

Figure 1: Example of a Continuum Spectrum after gain/offset correction, detector addition, and rebinning.

The 5 PCUs have similar, but not identical, gain. Since the high voltage is adjustable in steps of 20 V, individual gains can be adjusted in steps of about 15%. Several common data modes (the Standard modes and the Good Xenon modes, both of which maintain the detector identification) are processed with no on-board correction. Most modes, however, compress the data by selectively binning in time or energy, and usually add the data from the individual detectors together.

To minimize the energy smearing associated with co-added data, the EDS applies a gain and offset correction to the pulse heights from each detector. This is an integer arithmetic calculation which maps the 256 input channels into 256 corrected channels. The algorithm does no interpolation; when the gain is stretched, some of the corrected channels are empty and when the gain is compressed some of the corrected channels recieve data from 2 channels. The algorithm used by the EDS (implemented in integer arithmetic) is

$$\mathrm{J} = \frac{(\mathrm{I} \times (256 + G) + 128)}{256} + O \qquad (1)$$

where I is the pulse height produced by the PCU, J is the corrected pulse height, G is the commanded gain, and O is the commanded offset. The history of commanded values for G and O is given in Table 1. No gain and offset correction was applied beginning on January 18, as a bug in the flight software, which mapped some

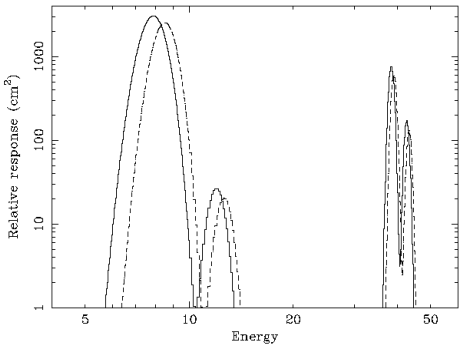

Figure 2: Relative response of 2 adjacent channels.

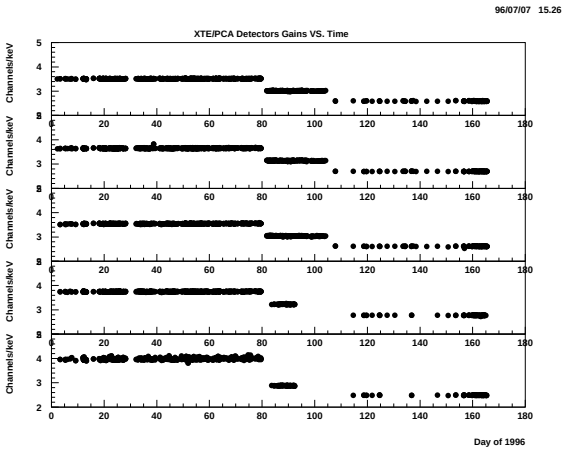

Figure 3: The number of channels per keV as a function of day of 1996. Except for high voltage changes, the gain is stable.

high pulse height channels (I) to low channels (J), was discovered. Gain correction was reenabled, with corrected software, on February 27.

Because the detectors have different corrections, and because all of the modes add several channels together, there are no empty channels after detectors are co-added. However, adjacent channels in a 64 channel spectrum contain different numbers of uncorrected channels. The generation of response matrices takes this into account; continuum models are predicted to have more or less counts per channel in the same manner as the data. Figure 1 shows the spectrum of a burst from J1744-28 from 1996 June 2 fit to a power-law model which illustrates this. The spectrum is plotted in channel space; the large step near channel 11 is where more uncorrrected channels are combined; this feature disappears when the same spectrum is plotted against an energy axis (fig 15). Figure 2 shows the relative response for two adjacent channels between 8 and 10 keV. Because one of the telemetered channels contains a larger number of *uncorrected* pulse height channels (I) after gain correction, summing over 5 detectors, and rebinning, these adjacent channels have responses that are different by 20%. Note that both channels have a contribution from the photopeak, and from L and K escape peaks from higher energy photons. [1]

[1] We have chosen to account for these differences in the effective area rather than in the reported channel width. Although the display is rougher, this is a more natural way to account for the channel rebinning in the environment of a spectral response modelling program such as XSPEC[5] which is supported by the RXTE Guest Observer Facility

Communication with the EDS (i.e. scientific data identification, gain and offset parameters) uses the 0-4 numbering scheme for the PCUs while communication with the PCA (i.e. high voltage commanding, housekeeping parameters) uses the 1-5 convention. We attempt to refer to PCU number in the "appropriate" scheme. (See for instance tables 1 and 2.)

3 OPERATIONS

The PCA operated flawlessly for the first 70 days in orbit. In mid March two of the five detectors showed occassional evidence of gentle breakdown.[2] These events are characterized by an increased count rate on some layers, are often accompanied by a spike in the count rate at the onset of the event, and result in a gain reduction by about a factor of 2 on some layers. In every case observed so far the gain reduction has occurred on both the veto anode signal chain and one of the main signal chains. Four operational changes were implemented in March and April 1996 to minimize the chances of further occurrences and to minimize the amount of time spent operating in the anomalous condition.

(1) We lowered the gain by 35% on all detectors. This was done in two steps as shown in figure 3 which

[2] We use gentle only in the sense that the on board High Rate Monitor did not inhibit these events.

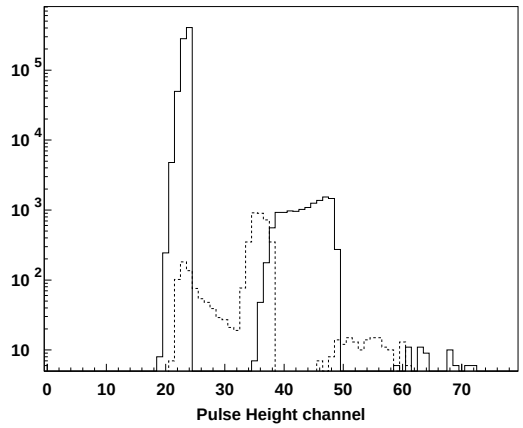

Figure 4: L1 and no-flag pulse height spectra for 8000 Hz input on L1.

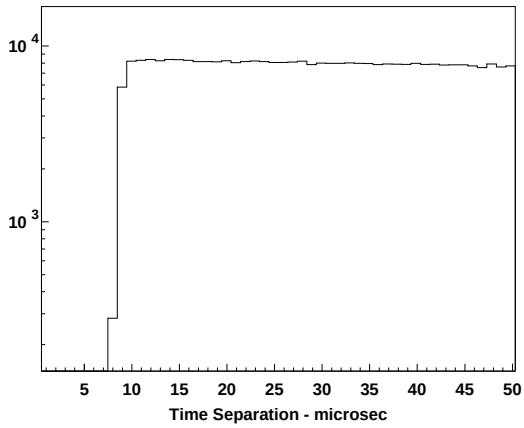

Figure 5: The distribution of time intervals between adjacent events. These data were collected with all input on layer L1.

plots the mean energy to channel conversion as determined from the on board calibration source. Aside from the obvious discontinuites corrsponding to commanded high voltage changes, the gain is quite constant. The effective dates of the high voltage commands are given in table 2. The net change on PCU 5 was 60 V, compared to 40 V on the other detectors; the result is that this detetor now has the lowest gain rather than the highest.

(2) We operate the detectors warmer, as the two detectors in question run at the coldest temperatures and our laboratory experience indicates that it is easier to induce breakdowns at colder temperatures. This is accomplished in three ways. (a) The spacecraft is now routinely oriented with 8° roll to increase the solar flux incident on the detectors. (b) The spacecraft reaction wheels are run at a higher speed to generate more heat. (c) We now schedule unconstrained observations (i.e. those which are not part of simultaneous observation/multi wavelength campaigns) to be done when the target is between $30° - 70°$ from the sun.[3] These orientations also increase the solar flux incident on the detectors. This combination of procedures generally keeps the coldest detector warmer than 0.5° C.

(3) We have implemented a real time gain monitoring system through the EDS and spacecraft Telemetry Status Monitoring system. The EDS takes advantage of the nearly identical response of the left and right anode chains on each signal layer[3] and calculates the first moment of the observed spectrum every 16 seconds. When the ratio of paired first moments is outside the range $0.6 - 1.5$, a signal condition is set. The spacecraft samples this signal and places it in telemetry every 8 seconds; if the signal is set for 5 consecutive intervals the spacecraft executes a stored command sequence that turns off the detector in question. The wide band of acceptable ratios assures that Poisson fluctuations during observations of faint sources will not set the trigger. This method and the adopted trigger criteria have neither failed to catch anomalous behaviour nor resulted in spurious turn offs. A detector experiencing the gain anomaly is therefore turned off within a minute of the onset of the anomalous behaviour.

(4) We now turn the high voltage to 0 V during passes through the South Atlantic Anomaly (SAA). At the beginning of the mission we reduced high voltage to $\sim$ 1000 V, i.e. well below the multiplication threshold, during SAA passage. However, events were still recorded as the charge generated by particles traversing the detector was still collected at the anode. To the extent that some of the interactions break apart molecules of the methane quench gas, it is possible that we were increasing the liklihood of an organic molecule buildup on the anodes. Removing the high voltage altogether does not reduce the number of molecules damaged by radiation, but it becomes unlikely that these molecules will become attached to the small surface area of the anodes.

[3] About 50% of the proposals accepted in response to the first NASA Announcement of Opportunity were not time constrained in any way.

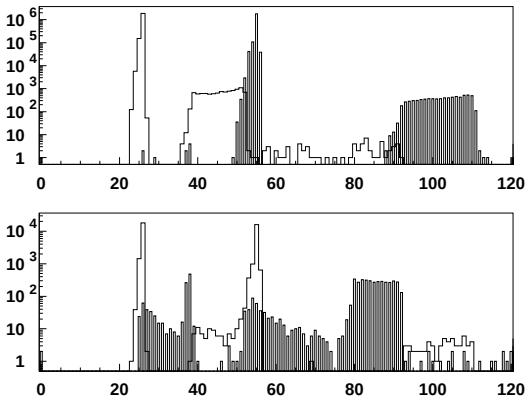

Figure 6: The pulse height distributions for L1 and R1 (top); 2-flag and no-flag (bottom).

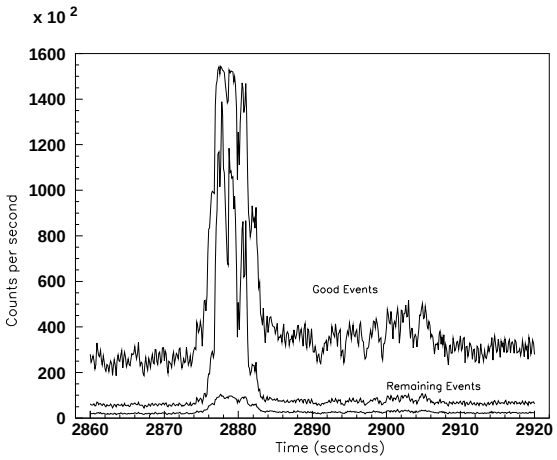

Figure 7: Rates during burst and good rate vs remaining rate

Between the end of April when all of these systems were operational and the end of June, there were 15 instances of the anomalous behaviour in PCU 4 and 3 instances in PCU 5. There is a suggestion that the PCU 4 anomaly is quasi periodic with a period near 3 days. We are currently (early July) operating detector 4 and 5 during observations which require large aperture and turning them off during observations which will be limited by cosmic background fluctuations or systematics in the background substraction in an attempt to learn whether the frequency of breakdowns can be reduced by introducing periods where the detectors can rest for several hours.

Even with the additional constraints described above, the PCA is supporting all of the peer reviewed and approved multi-wavelength observations and phase dependant monitoring campaigns, as well as numerous Target of Opportunity observations.

4 TIMING LOGIC

The low power filter design associated with each shaping amplifier produces a semi gaussian pulse with a 3μs peaking time and a $\sim 10\mu$s dwell time. Each layer generates a discriminator signal with duration 6μs when the LLD is exceeded. When the peak of the signal is detected (typically $\sim 3\mu$s later), and if the system is not busy, the peak is sampled and held, the system sets a busy signal and initiates the analog to digital conversion. About 2.5μs after the initiation of the system busy signal all of the LLD flags are latched for transfer to the EDS. In the case of a good event, only the flag that initiated the conversion is present.

We illustrate important features of the timing windows with ground data. Using a monochromatic tail pulse generator with randomly spaced pulses input on the L1 chain we obtained the pulse height spectrum shown as a solid line in figure 4. The pulse pile-up peak is obvious and a hint of a three-fold pile-up peak is seen. There is a small timing window during which an event can be analyzed and passed to the EDS without any LLD set. The dashed line is the pulse height spectrum for these *no flag* events. Because of the setup, we can be certain that these events were incident on L1. We can also identify that some of the unflagged events are in the pile-up and three-fold peaks. The rate in the L1 histogram is 7393 Hz, with 126 Hz in the pile-up peak; The no flag rates are 7.0 Hz (below channel 31) and 33.5 Hz in the pile-up peak. There is an obvious relationship between the unflagged and flagged pile-up events. Most events have the L1 flag and appear in channel 24; some events appear in channels 20-23 as these events began before the baseline restoration was complete. [4] Events that occur simultaneously produce a single flag, and the measured pulse height (channel 48) is twice the individ-

[4] This data over-emphasizes this effect for 2 reasons: the baseline restoration is optimized for X-ray pulses rather the test pulser, and the pulser signal is much narrower than the instrument resolution so that this effect is much harder to see for X-ray lines.

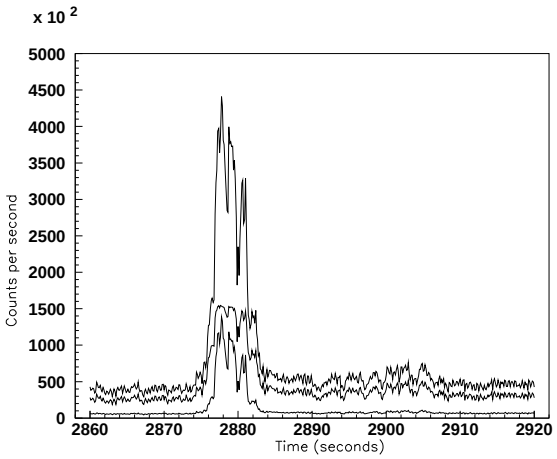

Figure 8: Lower limit to the total event rate in fig. 7 along with good and remaining rates.

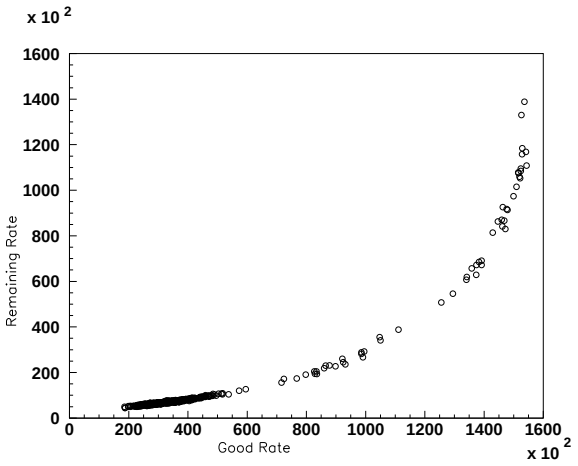

Figure 9: Remaining rate vs Good rate for a burst from J1744-28. The observed Good rate is near saturation, and accounts for less than one third of the photons incident on the PCA.

ual events. As the separation between the two events is increased up to $\sim 2\mu$s, there is still a single flag, but the peak is the sum of two misregistered events so that the summed pulseheight is less than 48. As the separation increases, the measured peak decreases and occurs later in time. Eventually the L1 discriminator pulse disappears before the peak is detected, resulting in an unflagged pile-up event. We use the relative integrals under the curves to calculate the windows for the various conditions below.

Figure 5 shows the distribution of time intervals between subsequent events. No pairs of events are processed with intervals smaller than 8μs; the system deadtime is $\sim 9\mu$s. The presence of some 8μs separations has to do with the measurement of an asynchronous process by counting an integer number of synchronous time steps.

We estimate the input rate in 2 steps. Summing the single and pile-up events (ignoring the triple pile-ups) we have 7560 pulse heights per sec. If the (non paralyzable) ADC deadtime (9μs) is the only significant deadtime, the input rate at the ADC was 8113 Hz; the input rate on L1 was closer to 8285 Hz (correcting for the fraction of ADC events that included two input events). [5] We estimate $r_{pu} = r_{in}^2 \times \Delta t_{pu}$ where r_{in} is the input rate, r_{pu} is the pile-up rate, and Δt_{pu} is the length of the window in which two events must fall to produce a pile-up. The window to produce a flagged pile-up is therefore 1.8μs and the window to produce an unflagged pile-up is 0.5μs. This leaves 6.7μs during which the system is busy and the second event is lost. We predict 460 events per sec in this category. Adding the good event rate (7393), twice the pile-up rate (320), and the missed events (460) gives 8173 Hz, in approximate agreement with our estimate. Table 3 gives similar rates for several input pulse heights.

The same features are visible in figure 6 which shows the pulse height distributions for random pulsers, with different amplitudes, input on L1 and R1 in the top panel. The pulse height distribution for unflagged events is shown in the bottom panel (solid) along with the noflag pulse height. Here the measured R1 rates are 2021(10.3) for main peak (pile-up peak); the L1 rates are 1989(7.2). The total no-flag rate is 5.2 Hz. The 2 flag peak near channel 24 has a rate of 19.6 Hz while the peak near channel 52 has a rate of 18.0 Hz. The total rate of pulse height conversions is 4070 Hz, which implies that the input rate to the analog to digital converter was 4225 Hz and the incident rates on R1 and L1 were 2098 and 2065 Hz respectively. The pile-up windows on R1 and L1 (calculated as if independent) are 2.3 and 1.6μs (perhaps surprisingly different, although the L1 time agrees well with the values tabulated in table 3 derived from data on this signal chain.) Under the assumption that the 2 flag peak at channel 24 consists entirely of R1 events followed by L1 events, the window for such occurances is 4.5μs while the window

[5] The Crab nebula plus pulsar produce about 2600 counts per second, distributed over all 6 xenon signal chains.

for L1 events followed by R1 events is only 4.1μs . This is qualitatively understood. Since this experiment contained R1 events with smaller pulse height, the time between crossing the LLD threshold and the signal peak is smaller than for events on L1. Therefore, the discriminator pulse is held high longer into the analog to digital conversion period, increasing the window for 2 LLD flags. We are developing a program to simulate the PCA response to high rates that will eventually include the full energy dependence of all the timing windows. A description of that work, as well as a detailed treatment of predicting the Poisson level for PCA power density spectra in the presence of these deadtime processes and the VLE window, is being prepared separately.

Although most sources of interest to RXTE do not have large deadtime in the PCA (the example shown in figure 4 corresponds to the rate expected from a 5 Crab source), the brightest sources in the sky do cause unusual (i.e. beyond the typical textbook description) deadtime behaviour. The EDS typically sends data only from good (i.e. one LLD) events. For particularly bright sources, there is a significant signal contained in events which contain two (or more) LLD flags each of which corresponds to a cosmic X-ray. The bright transient source J1744-28 was originally observed with a non bursting count rate of $\sim 25,000$ Hz and bursts which reached 150,000 Hz. Standard 1 data, however, provides light curves at 0.125 second resolution of good events, propane events, and remaining counts (i.e. those events with a pulse height that contain no or two or more flags). Figure 7 shows measured rates during a burst observed on Feb. 4, 1996. From the top the curves give the total good rate, the remaining rate, and the propane rate. Figure 8 shows the remaining and good rates as well as a lower limit to the input rate constructed by adding the good rate and twice the remaining rate (assuming that this rate is dominated by double discriminator events). Note that the remaining rate is much more sharply modulated than the good rate, indicating that the good rate is near saturation. We show the same data in figure 9, plotting the remaining rate as a function of the good rate.

5 COLLIMATOR RESPONSE

The RXTE spacecraft was designed to ensure that the 5 PCA detectors (and the 2 HEXTE clusters) would be copointed within a circle of $\leq$ 6' radius. The achieved pointing directions of the 5 PCA detectors and 2 HEXTE clusters, as well as the science-axis, are given in table 4 in the spacecraft frame. The +X direction is close to the science axis; the ASM is mounted on the -Z side of the spacecraft. Most of the relative misalignment is along the spacecraft z-axis; the maximum distance (PCU 5 to HEXTE clusters) is $\sim$ 7'.

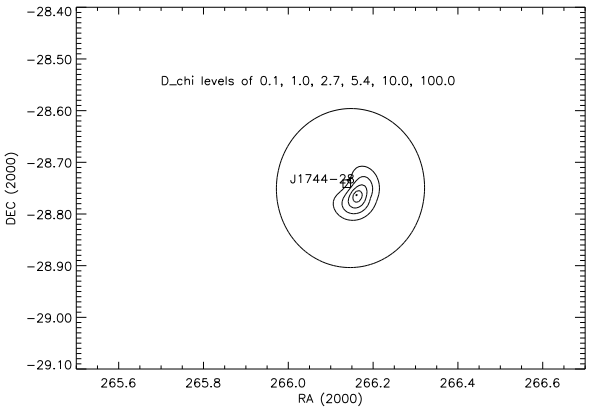

Figure 10: Chi-squared contours for the positions of a burst observed with the PCA. This burst is known to originate from J1744-28, marked by a square. Contours are show $\Delta\chi^2$ levels as indicated.

The misalignement of the PCA detectors can be useful for providing additional information about the position of bursts. A simple model, containing the peak pointing position of each detector, an assumed transmission that is the convolution of a perfect hexagonal collimator and a 6' FWHM gaussian, and current estimates of the relative effective areas of the 5 detectors can be used in conjunction with the 5 rates (from individual detectors) and the spacecraft pointing information to estimate the position of bursts. Figure 10 shows the chi squared contours derived for a burst detected during an observation of 1744-28 and the true position of the source. This burst is known to be associated with this source as it has significant power at the 2.1 Hz pulse frequency of 1744-28. Given the simplifications in the collimator transmission model, the agreement is perhaps better than expected. This analysis used data from 0.25 sec, and contains about 2000 counts from each detector. Type I X-ray bursts, of uncertain origin, were also observed during some observations of 1744-28. Because such bursts had not been previously observed, and because of predictions that they should be,[6] the capability of positioning bursts has been extremely valuable. Results from analysis similar are shown in figure 11, and indicate that this burst is unlikely to have come from

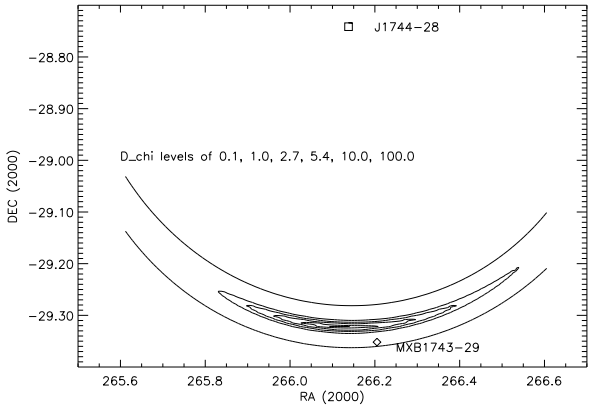

Figure 11: Similar analysis as 10, but for a burst that probably does not originate from J1744-28.

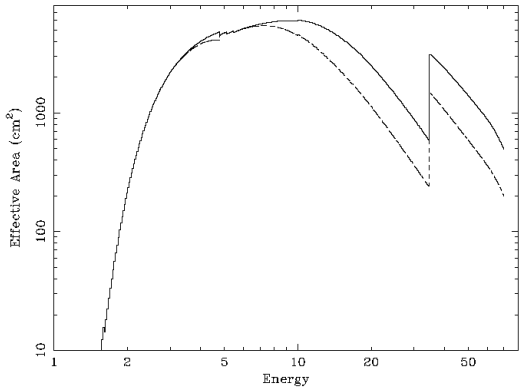

Figure 12: The upper curve shows the total effective area and the lower curve shows the effective area for the first layer only. Both curves are summed over 5 detectors.

1744-28. This analysis used 2 sec of data and about 4000 counts from each PCU. The model for positioning such bursts will be improved with data taken during the IOC period when numerous scans across the Crab pulsar plus nebula were performed for just this reason. The relative count rate per PCU also has a small spectral dependence, not yet included in our model.

6 ENERGY RESPONSE

The low energy threshold of the PCA is determined by the transmission of the two mylar windows (1 mil each) and the propane volume. The front volume contains $\sim 2.6 \times 10^{-3}$ gm cm^{-2} of propane. While on the ground a small amount of Xenon permeated the inner window of each detector, resulting in 1.1, 1.3, 1.5, 2.3, and 3.3×10^{-4}gm cm^{-2} of Xenon in the propane layers for PCU 1-5 respectively. These values were determined by assuming a value of 0, and fitting first layer data for the Crab, and allowing an edge at 4.78 keV. The values may change slightly once the matrix more accurately reflects behaviour near the Xenon edges. With the colder temperatures experienced on orbit (from $1-10°$ C) compared to most of the ground storage and testing ($20-25°$ C), the permeation of Xenon into the front volume has apparently ceased. The net effective areas of the total PCA is shown in figure 12, as well as the effective area for the first layer alone.

The gain has been stable over the first 6 months, except for discrete changes associated with changes to the detector high voltage. Figure 3 shows the number of channels per keV deduced from the Am^{241} calibration source for each of the 5 detectors. Additional information about the energy scale has been obtained from measurements of the Iron line in the super nova remnant Cassiopeia A, and the Xenon L escape peak which is collected in a special mode that keeps all events with a calibration flag. Some events of these events have a two fold coincidence, a fraction of these are L-escape events, and a for a fraction of these, the L escape photon, recaptured in a different signal chain, is pulse height analyzed. This data is collected periodically; about 3 hours are required to obtain enough Xe L photons for a significant fit. Figure 13 shows the calibration spectrum collected without regard to number of LLD bits set. The Xenon L-escape peak at 4.1 keV is not present in the data restricted to events with the calibartion flag and a single LLD which is routinely present in the Standard 1 data.

The energy to channel relationship is currently characterized by a quadratic fit to 7 lines: the Xe-L escape at 4.1 keV, the Cas-A Iron line at 6.57 keV,[7] and 5 lines from the Am^{241} calibration source. This approach leads to large residuals in the vicinity of the Xenon edges, particularly the L edge where the Poisson error is often vanishingly small. We have not yet included the known jumps at the edges which amount to about 90 eV at the L edge[8,9] and 180 eV at the K edge.[10,11]

Figure 14 shows the data from the front layer of PCU

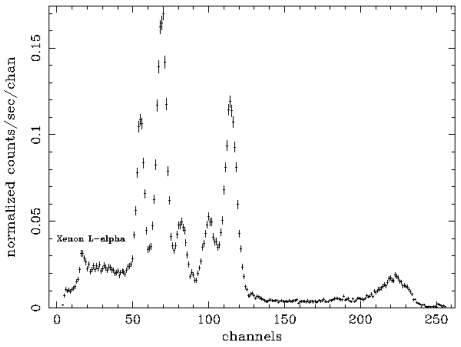

Figure 13: The pulse height spectrum from the calibration source including the Xenon L escape line.

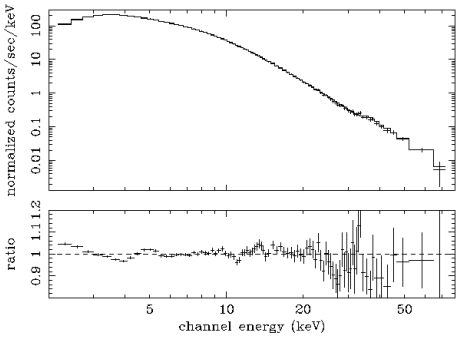

Figure 14: Data and power law model for the Crab. The lower panel shows the ratio of the data to the model.

0 from an observation of the Crab. The model is a powerlaw of photon index 2.08 and interstellar absorption (fixed) at 3×10^{21} Hydorgen atoms cm^{-2}. The lower panel shows the ratio of the data to the model; there is an inflection near the Xenon L edge and a similar inflection (not as visible due to decreased statistical precision) near the Xenon K edge, due to the discontinuities noted above. Recent work[12] provides measurements and Monte Carlo calculations of the number of electrons produced by photons absorbed in Xenon counters, which contains the information previously expressed in terms of a discontinuity. This information will be incorporated in the next version of the PCA response matrices.

Figure 15 gives a similar example with a harder spectrum, characterized by a photon index of 1.4 and an absorption column depth of $1 \times 10^{23}\,cm^{-2}$.

7 BACKGROUND

One of the key observational goals of the RXTE is the broad band measurement of spectra of Active Galaxies. Because these objects are relatively faint, sensitivity is limited by either photon counting statistics or systematics in the background estimation. Unlike HEXTE which rocks, and produces continuous measurements of the background (albeit at the cost of half of the potential on source exposure), the PCA relies on a model background. Such a scheme has been successfully used most recently for GINGA data[13] which was obtained from an experiment with a more variable background. Several features of the PCA instrument and RXTE mission design led to an expectation of a lower and less variable background. These were: (1) the counter bodies were constructed of aluminum rather than steel. The low Z material is less subject to activation and has a lower interaction cross section for interactions with particles or γ-rays. Each PCU also has a graded shield constructed of Tin and Tantalum.[2,3] (2) The RXTE orbit is circular, which removes the term present in the GINGA model[13] which accounted for the precession of the orbit and the variable average time spent in the SAA. (3) The RXTE orbit is lower inclination (23° vs 31°) so that RXTE spends less time in the SAA. (4) Each PCU has a front propane layer which helps reduce the background due to electrons. The presence of the propane layer and the need for two windows results in a higher low-energy threshold. (5) The RXTE spacecraft provides a sunshield which prevents direct solar illumination of the thermal shield. For sun angles $\geq 40°$ singly scattered solar X-rays are completely eliminated.

7.1 Level and Variability

Figure 16 shows the total background summed over all 5 PCU detectors during the In Orbit Checkout observations of NGC 4151, as well as the background for the sum of the first layers only. Line features are present due to Xenon L escape photons, Copper fluoresence (primarily from the backplane, and concentrated in the third

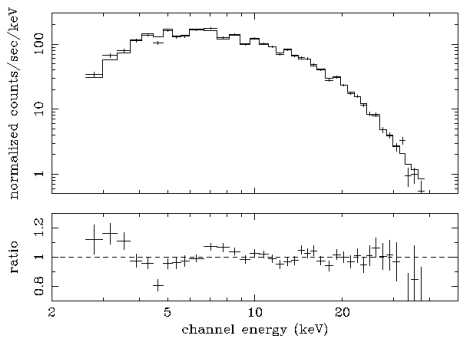

Figure 15: Energy spectrum of a burst from J1744-28. These are the same data as fig 1.

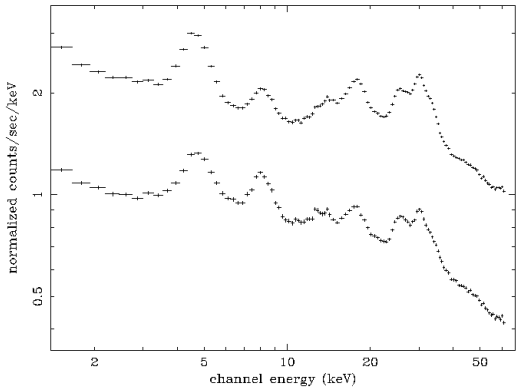

Figure 16: The total and first layer only background for PCA observations of the earth.

layer), unflagged calibration events, and a contribution which appears to come from residual activity in the collimator. The net observed rates, which are quite similar to the pre-launch predictions, are tabulated in 3 broad bands in table 5; the table lists the sum over the entire PCA and for a single detector. The background typically varies between 18-24 cts/s/PCU, and most of the variability is tracked by rates which measure multiple coincidences between anode chains and which measure instantaneous ionizing particle flux, primarily protons. Figure 17 shows the relationship between total rate and 6 fold coincidences; while there is a strong correlation it is also clear that a small fraction of the data is sensitive to (at least) one other parameter not tracked by the coincidence rate.

7.2 Background Model status

The simplest model of the background is a one parameter model of the background rate. We have created such a model, using the 6 fold coincidence rate as the measure of background. We bin data from 90 ksec of earth viewing data obtained during the first 60 days of operation by the measured coincidence rate. We then estimate the instantaneous background (with 16 sec resolution) by interpolating between the measured earth viewing spectra in the bins which bracket the instantaneous particle rate. Figure 18 shows the measured and predicted rates above 20 keV, summed over 5 detectors, for one orbit during IOC when RXTE was viewing blank sky. The contribution of the Cosmic X-ray Background is expected to be small in this band. The predicted background rate tracks the observed rate well, and in particular reproduces a variation with a time scale of 1000 sec near the center of the interval. The background model falls slightly below the observed level at the beginning and end of this stretch, indicating a need for a second parameter or stricter data selection criteria; we are exploring both possibilities. The sum of the predicted background is 98.7% of the observed background in this energy range integrated over this orbit.

Acknowledgements. This work would not have been possible without the dedicated help of colleagues too numerous to mention individually. We thank our collaborators in the GSFC Laboratory for High Energy Astrophysics, the MIT Center for Space Research, the GSFC Engineering and Flight Projects Directorates, and the RXTE Science Operations Center.

8 REFERENCES

[1] Swank, J. H. et al. *The Lives of Neutron Stars*, M. A. Alpar et al. eds., NATO ASI Series, (Kluwer:Doordrecht) 1994.

[2] C. A. Glasser, C. E. Odell, and S. E. Seufert, *IEEE Trans. Nucl. Sci.* NS-41(4), 1343, August 1994.

[3] W. Zhang et al. *Proc. SPIE* 2006, 324, July 1993.

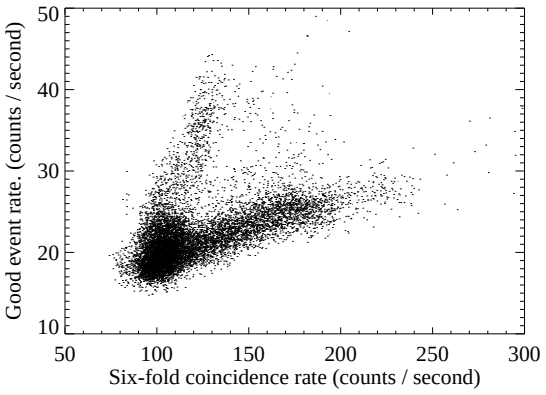

Figure 17: The total good event rate as a function of the six fold coincidence rate, which tracks the particle flux.

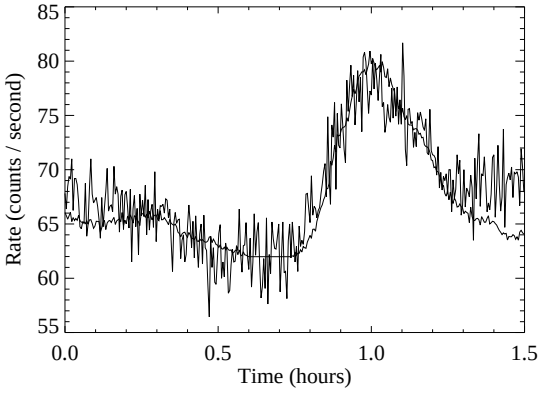

Figure 18: Measured (thin line) and predicted (thick line) rates above 20 keV summed over all 5 PCU detectors.

[4] Table Ap.1.3, *Appendix F: The XTE Technical Appendix*, ftp://legacy.gsfc.nasa.gov/xte/nra/appendix_f/global/chap11appen1.ps

[5] Arnaud, K. A. "XSPEC: The First 10 Years", *Astronomical Data Analysis Software and Systems, V.* eds. G. Jacoby and J. Barnes, in press.

[6] L. Bildsten and E. Brown, "Thermonuclear Burning on the Accreting X-Ray Pulsar GRO J1744-28", *Ap. J. Lett.* submitted.

[7] S. S. Holt et al. "ASCA Observations of Cassiopeia A", *Publ. Astron. Soc. Japan*, 46, L151, 1994.

[8] J. M. F. dos Santos et al. "The Energy Linearity of Gaseous Xenon radiation Detectors for X-rays", *Nucl. Instrum. Meth.*, A324, 611, 1993.

[9] M. Bavdaz et al. "The Spectroscopic Capabilities of Imaging GSPCs", *Proc. SPIE 2518*, 1995.

[10] J. M. F. dos Santos et al. "The energy Nonlinearity of a Xenon GSPC at the K-absorption Edge in Xenon", *Nucl. Instr. Meth.*, A350, 216, 1994.

[11] H. Tsunemi et al. "Nonlinearity at the K-absorption Edge in Xe-filled Gas Proportional Counter", *Nucl. Instr. Meth.*, A336, 301, 1993.

[12] F. P. Santos et al. "Variation of Energy Linearity and w-value in Gaseous Xenon Radiation Detectors", *Nucl. Instr. Meth.*, A307, 347, 1991, and J.M.F. dos Santos, personal communication.

[13] Hayashida, K. et al., "On the Origin and Behaviour of the Background in the GINGA LAC", *Pub. Astron. Soc. Japan*, 41, 373, 1989.

Table 1: Gain and offset values

Effective Date	PCU 0-4 Gain coefficient	PCU 0-4 Offset coefficient
95 Dec 30:14:00:00	24 22 29 10 2	1 1 1 0 0
96 Jan 18:18:31:44	0 0 0 0 0	0 0 0 0 0
96 Feb 27:19:24:39	29 20 27 14 -1	-1 -1 -1 -1 -1
96 Mar 25:21:02:50	29 20 27 14 33	-1 -1 -1 -1 -1

Table 2: High voltage changes

Effective Date	PCU 1-5 Xenon High Voltage
95 Dec 30:14:00:00	2030 2030 2026 2027 2048
96 Mar 21:18:33:40	2010 2010 2006 2007 2007
96 Apr 15:23:06:00	1990 1990 1986 1987 1988

Table 3: Timing windows for Single Anode Chain

ch	$L1$	$L1_{pu}$	$N.F.$	$N.F._{pu}$	Input	Δt_{pu}	$\Delta t_{pu}(nf)$	Δt_{busy}	Sum
8	7514	28	4	-	8126	0.4	0.0	8.6	8138
16	7085	44	6	20	7715	0.7	0.3	8.0	7689
24	7394	126	7	34	8285	1.8	0.5	6.7	8174
32	7639	116	9	42	8566	1.6	0.6	6.8	8554
42	7372	111	9	46	8254	1.6	0.7	6.7	8142
50	7395	107	10	49	8280	1.6	0.6	6.8	8173

Table 4: Peak transmission directions in Spacecraft Coordinates

	Y	Z
PCU 1	-0.00024	0.00070
PCU 2	-0.00010	0.00060
PCU 3	-0.00026	0.00082
PCU 4	0.00010	0.00138
PCU 5	0.00010	0.00202
HEXTE 1	0.00002	0.00020
HEXTE 2	-0.00003	-0.00005
Science Axis	0.00000	0.00070

Table 5: Background Count Rates

Band	2 - 10 keV	10 - 30 keV	30 - 60 keV
PCA - total	17.20	39.20	39.70
PCA - first layer	8.50	17.00	16.60
PCU 0 - total	3.29	7.55	7.48
PCU 0 - first layer	1.61	3.30	3.16